International Journal of Automotive Technology, Vol. 8, No. 2, pp. 193−201 (2007)

Copyright © 2007 KSAE
1229−9138/2007/033−08

NUMERICAL SIMULATION OF CONVEX AND CONCAVE TUBES WITH CONSIDERATION OF STRAIN RATE SENSITIVITY

B.-W. YE[1)*], S. OH[1)], Y.-B. CHO[2)] and H.-C. SIN[1)]

[1)]School of Mechanical and Aerospace Engineering, Seoul National University, Seoul 151-744, Korea
[2)]TNO Automotive Korea Ltd., Rm 1810, LG Twintel 2, 157-3 Samseong-dong, Gangnam-gu, Seoul 135-880, Korea

(Received 2 May 2005; Revised 23 January 2006)

ABSTRACT−The present paper deals with the application of the explicit finite element code, PAM-CRASH, to simulate the crash behavior of steel thin-walled tubes with various cross-sections subjected to axial loading. An isotropic elastic, linear strain-hardening material model was used in the finite element analysis and the strain-rate sensitivity of mild steel was modeled by using the Cowper-Symonds constitutive equation with modified coefficients. The modified coefficients were applied in numerical collapse simulations of 11 types of thin-walled polygon tubes: 7 convex polygon tubes and 4 concave polygon tubes. The results show that the thin hexagonal tube and the thick octagonal tube showed relatively good performance within the convex polygon tubes. The crush strengths of the hexagonal and octagonal tubes increased by about 20% and 25% from the crush strength of the square tube, respectively. Among the concave tubes, the I-type tube showed the best performance. Its crush strength was about 50% higher than the crush strength of the square tube.

KEY WORDS : Numerical simulation, Crush strength, Strain rate effect, Axial collapse

1. INTRODUCTION

To understand the crash behavior of a complex structure such as a vehicle, one must first acquire an understanding of the crash characteristics of structural elements that constitute the system and control their crash performances. One of the most important characteristics in the design of structural elements for crash energy management is the load-carrying capacity or strength under various types of loadings and the associated modes of collapse that will affect the energy dissipation of these elements (Mahmood and Paluszny, 1981). The front rail can absorb as much as 85% of the energy of a body-on-frame vehicle in a full-vehicle crash (Gonzalez *et al.*, 2005). Accordingly, if the frontal crash members absorb more collision energy, crashworthiness of the whole vehicle will improve greatly.

Abramowicz and Jones (1984) conducted 84 dynamic tests on thin-walled square tubes having two different cross-sections. The square tubes were crushed axially on a drop hammer rig.

Outbushin (1998) modeled the strain rate sensitivity of mild steel by using the Cowper-Symonds constitutive equation with modified coefficients. Abramowicz and Jones (1984) suggested D=6844/s and p=3.91 as coefficients in the finite element analyses of materials undergoing large deformations.

**Corresponding author.* e-mail: mokgok@empal.com

Abramowicz and Wierzbicki (1989) observed that the crush resistance, or energy absorption, of a thin-walled column depends heavily on both the angle between adjacent plates and the number of corners.

Kang and Huh (2000) constructed the Johnson-Cook equation as the constitutive relation from experimental results of static and dynamic tests with a tension split Hopkinson bar apparatus. The Johnson-Cook equation was applied to simulations of the dynamic behavior of auto-body structures.

Kim *et al.* (2002) constructed a horizontal impact testing machine to estimate the absorbed energy abilities with using a controller and a method to measure the load and the displacement diagram during crushing was considered. The energy absorbing capacity of Al tubes were estimated with-controller and without-controller, respectively based on height, thickness, clearance of a controller.

Yamashita *et al.* (2003) investigated the effect of the cross-sectional shape on the crush behavior with respect to the deformation pattern and crush strength. They used the explicit finite element code of the public domain version of DYNA3D. They suggested that crush strength increases as the number of corners in the cross-section increases. The effect of the number of polygonal corners on enhancement of crush strength became more prominent as the initial wall thickness decreased. Strain-rate dependency was not considered in their study, however.

Mamalis *et al.* (2003) simulated the crash behavior and

energy absorption characteristics of steel thin-walled tubes with octagonal cross-sections subjected to axial loading using the commercial explicit finite element code LS-DYNA.

Rossi *et al.* (2005) dealt with the post-buckling deformation characteristics of aluminum alloy extruded polygonal section tubes subject to dynamic axial impacts by using LS-DYNA. The increase in the number of walls (flanges) directly affected the mean axial crushing force and the values of the permanent displacement parameters. The adoption of a hexagonal tube section as an axially loaded energy absorbing column yielded an average increase of 11% in the mean axial crushing force and an average decrease of 10% in the permanent displacement.

Gonzalez *et al.* (2005) showed that geometry, material properties, forming effect, welding effect and strain rate all contributed to their CAE model correlation. The comparison of the hexagonal and octagonal tubes showed that the octagonal cross section was slightly more advantageous in terms of energy absorbing capability in axial crushes.

The interest taken in the use of multicorner thin-walled tubes is concerned with the lightweightness of vehicles. Various ideas to use less material but obtain sufficient crashworthiness have been proposed to attain this objective.

The present paper deals with the application of the explicit finite element code, PAM-CRASH, to simulate the crash behavior of thin-walled steel tubes with various cross-sections subjected to axial loading. In section 2, the simulations were validated against the experimental results of Abramowicz and Jones (1984), which were obtained from a series of drop-hammer tests in which two different cross-sections with thickness to side length ratios of 0.031 and 0.033 were struck axially. In our finite element analysis, an isotropic elastic, linear strain-hardening material model was used, and the Cowper-Symonds constitutive equation was used to consider the strain rate sensitivity. The coefficients D and p in the equation were determined by the experimental results.

In section 3, the coefficients obtained were applied in the numerical collapse simulation of 11 types of polygon tubes: 7 convex polygon tubes and 4 concave polygon tubes. The circumference and thickness of the tubes were made to be equal so that only the effect of multiple corners in the cross-section could be examined and compared. Many researchers have conducted extensive simulation studies on the collapse of convex polygon tubes. The crush strength increases as the number of corners in the cross-section increases. Therefore, the purpose of the present study is to show how the crush strength changes with an increase of the number of corners in the cross-section for concave polygon tubes. The crush strength of the concave tubes is expected to be higher than that of the convex tubes because the volume efficiency is better than those of the convex tubes. Notably, an I-type tube has the highest crush strength among the various types of tubes in the present study.

2. VERIFICATION OF THE MATERIAL MODEL

2.1. Experimental Data

In the 84 drop-hammer experiments reported by Abramowicz and Jones (1984), various masses were dropped onto square cross-section mild steel specimens that were resting on a rigid platen. Specimen I21 had a side length of 37.07 mm, a nominal wall thickness of 1.152 mm and a longitudinal length of 244.1 mm. The drop-hammer mass was 73.6 kg and the initial velocity of the drop-hammer was 10.288 m/s.

Static tensile tests were performed on the coupons cut from the undeformed specimens in the same batch at a strain-rate of approximately 2×10^{-4}/s. Results from the tensile tests of specimen I21 gave an average value of 277.5 MPa for the 0.2% proof stress, 330.5 MPa for the ultimate stress and 161 MPa for the hardening modulus.

Specimen 22 had a side length of 49.31 mm, a nominal wall thickness of 1.63 mm, and a longitudinal length of 244.4 mm. The drop-hammer mass was 73.6 kg and the initial velocity of the drop-hammer was 10.097 m/s. Results from the tensile tests of specimen 22 gave an average value of 264.5 MPa for the 0.2% proof stress, 328.5 MPa for the ultimate stress and 165 MPa for hardening modulus.

Table 1 shows the data from the verification models and the results of the drop-hammer tests from Abramowicz and Jones (1984). In Table 1, c is the side length of tubes, t is the thickness, L is the longitudinal length, M is the collision mass, V is the impact velocity and K is the kinetic energy. δ_f is the crushed distance of the tube and P_m^d is the dynamic mean crush load. In the paper by Abramowicz and Jones (1984) the dynamic mean crush load was defined as kinetic energy divided by crushed distance.

An isotropic elastic, linear strain-hardening material model was used to represent the specimens with a Young's modulus 200 GPa and Poisson's ratio 0.3.

In dynamic analysis, the strain rate effect should be included in constitutive relations if the strain rate is considerably high. The simplest constitutive equation that

Table 1. The data from the verification models.

	c (mm)	t (mm)	L (mm)	M (kg)	V (m/s)	K (kJ)	δ_f (mm)	P_m^d (kN)
I21	37.07	1.152	244.1	73.6	10.288	3.90	149.5	26.1
22	49.31	1.63	244.4	73.6	10.097	3.75	82.1	45.7

considers the strain rate effect is the Cowper-Symonds equation. The following empirical Cowper-Symonds uniaxial constitutive equation is widely used to assess material strain rate effects in structures.

$$\frac{\sigma_y^d}{\sigma_y}=1+\left(\frac{\dot{\varepsilon}}{D}\right)^{\frac{1}{p}} \tag{1}$$

where σ_y^d is the dynamic yield stress, σ_y is the initial yield stress, $\dot{\varepsilon}$ is the strain rate and D and p are the Cowper-Symonds strain rate parameters.

Outbushin (1998) conducted finite element analysis by using the coefficients D=6844/s and p=3.91. The results of the finite element analysis with these coefficients were, however, much different from the experiment results of Abramowicz and Jones (1984), so we obtained the values of D and p that would yield approximately the same results as the experimental results.

2.2. Tube I21

Outbushin (1998) introduced geometric imperfections in the form of nodes displaced 0.5 mm out of plane in consideration of the expected mode of collapse. Two nodes on opposite sides of the specimen were altered before the main analysis. When there were no geometric imperfections, sequential folding did not occur.

Figure 1 displays how the crushed distance changes depending on the Cowper-Symonds' coefficients. The result of the simulation using the coefficients used by Outbushin (1998) was found to be in error by 28% compared to that of the drop-hammer experiment. When the strain rate effect was not considered, the error reached up to 39%. The crushed distance from the simulation result with the Cowper-Symonds' coefficients D=300/s and p=4 was close to that of the experiment. When the coefficients, D and p, were 300/s and 5 respectively, the simulation result also came close to the experiment; but when D was changed to 400/s while p was kept at 5, the change of the crushed distance became 15 mm, which is three times of an increase compared to the result when p was 4.

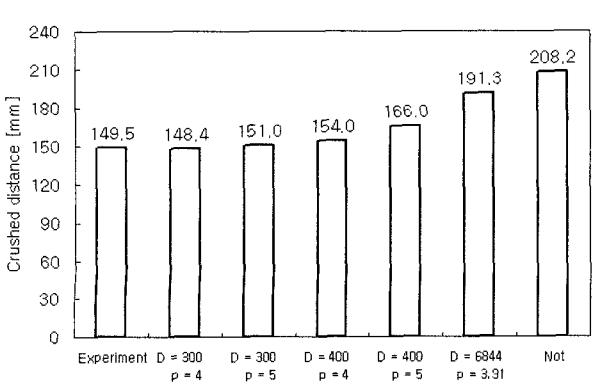

Figure 1. Crushed distance of Tube I21.

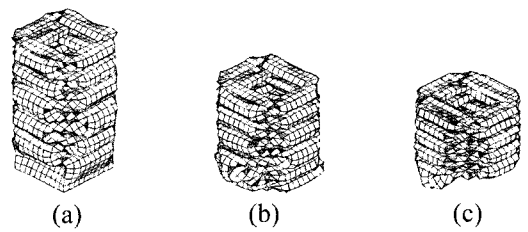

Figure 2. Final collapse mode of Tube I21: (a) D=300/s, p=4; (b) D=6844/s, p=3.91; (c) No consideration of the strain rate effect.

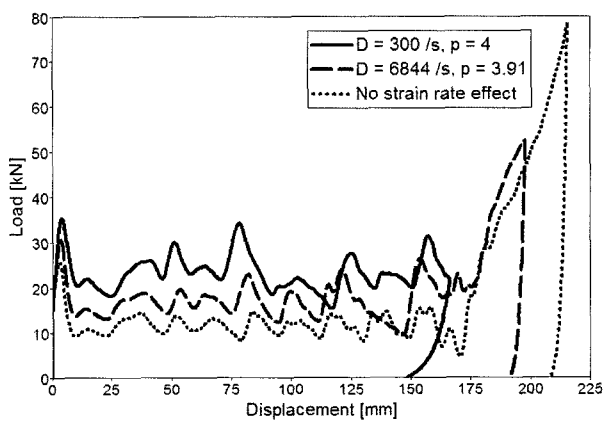

Figure 3. Rigid wall force of Tube I21 with crushed distance.

Therefore, we used the coefficients D=300/s and p=4 in the simulations when about 5/8 of the whole tube length collapsed.

Figure 2 shows the final collapse shape of Tube I21. The collapse in (b) and (c) occurred excessively. In the collapse process, the stiffness increases when the strain rate is high, and as a result, less folding occurs. The crush strength of Tube I21 was 153 MPa, which was obtained from dividing the mean crush load, 26.1 kN by the cross-sectional area of Tube I21, 170.8 mm^2.

Figure 3 is a graph that displays the rigid wall force of Tube I21 for different crushed distances. The mean crush load rises as the crushed distance becomes shorter. The area under each graph is the internal energy that Tube I21 absorbed for each case. In the three curves of the rigid wall force in the figure, the areas are almost the same because the collision energy is the same.

2.3. Tube 22

The conditions in Table 1 were used for the simulation of Tube 22. The geometric imperfections were introduced so that sequential folding could occur as it did in Tube I21. Because the cross-sectional area of the tube is increased compared to Tube I21, the dynamic mean crush load was expected to increase. The comparison of the results in

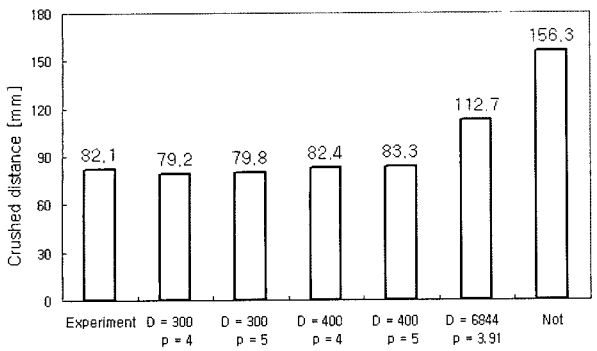

Figure 4. Crushed distance of Tube 22.

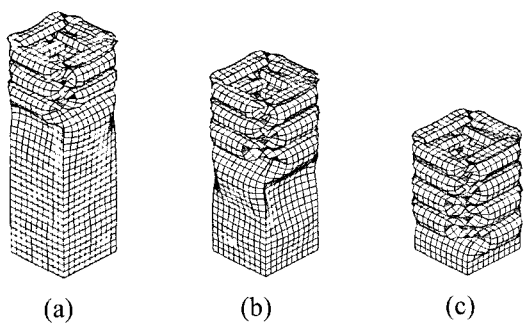

Figure 5. Final collapse mode of Tube 22: (a) D=400/s, p=4; (b) D=6844/s, p=3.91; (c) No consideration of the strain rate effect.

Figures 3 and 6 clearly shows this increase in the dynamic mean crush load.

Figure 4 displays the crushed distance versus the material properties of Tube 22. Since the collapse became slower due to the increase of the cross-sectional area, the coefficient D was adjusted to a larger value than that used for the case of Tube I21. The crushed distance from the simulation result with the Cowper-Symonds' coefficients D=400/s and p=4 agreed with the experiment. So, we used the coefficients D=400/s and p=4 in the simulations when the tube length collapsed to about 1/3 of the original.

Figure 5 shows the final collapsed shape of Tube 22. The tube with no strain rate effect taken into consideration folded excessively. Figure 5(a) displays the result of the simulation that agrees fairly well with the experiment when D=400/s and p=4. As previously stated, the stiffness increases for the high strain rate, resulting in little folding. Figure 6 is a graph that displays the rigid wall force of Tube 22 for different crushed distances. The mean crush load with D=400/s and p=4 is nearly two times larger than that for the case without consideration of the strain rate effect. The crush strength of Tube 22 is 142 MPa, which is again obtained by dividing the mean crush load, 45.7 kN, by the cross-sectional area of Tube 22, 321.5 mm^2.

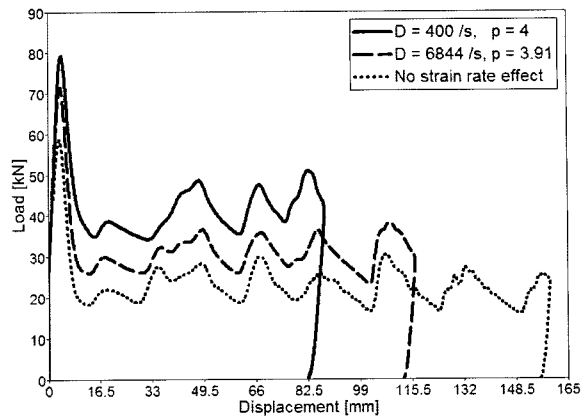

Figure 6. Rigid wall force of tube 22 with crushed distance.

2.4. Square Tubes that Have Large Section Size

The coefficients obtained are applied in the simulation of square tubes that have a large section size. The section size is 100 mm × 100 mm. The crush strength functions are used to verify the crush strength of the large tubes. The static crush strength of square tubes is a function of the ratio of the thickness to the side length and yield stress. The dynamic crush strength is a function of the static crush strength and impact velocity.

Mahmood and Paluszny (1981) suggested the following static collapse equation for square tubes:

$$\sigma_{CS}^{s}=96.2(t/c)^{0.86}\sigma_y^{0.57}\beta^{-0.43} \tag{2}$$

$$\beta=14.085\times t/c+0.7746 \quad (0.016<t/c<0.038) \tag{3}$$

where, $\sigma_{CS}{}^{S}$ is the static crush strength and β is plasticity hardening which is a function of the t/c ratio. Since the yield stress of Tube I21 is 277.5 MPa, the static crush strength is 108 MPa. Also, when the t/c ratio is 0.033, the static crush strength is 113 MPa because the yield stress of Tube 22 is 264.5 MPa.

Abramowicz and Wierzbicki (1989) also suggested a static collapse equation for square tubes as follows:

$$\sigma_{CS}^{s}=\frac{1}{4ct}P_{ms}=\frac{1}{4ct}55.22(t/c)^{-1/3}M_o \tag{4}$$

$$M_o=\frac{1}{4}\sigma_0 t^2 \text{ and } \sigma_0=0.92\sigma_u \tag{5a, b}$$

where P_{ms} is the static mean crush load, σ_0 is flow stress, and σ_u is ultimate tensile stress.

The static crush strengths of Tube I21 and Tube 22 calculated by equation (4) were 103.7 MPa and 107.4 MPa because the ultimate stress of Tube I21 and Tube 22 were 330.5 MPa and 328.5 MPa, respectively. The experimental results of Abramowicz and Jones (1984) were 122 MPa and 110 MPa, respectively. Because Tube I21 folded asymmetrically in the quasi-static compression

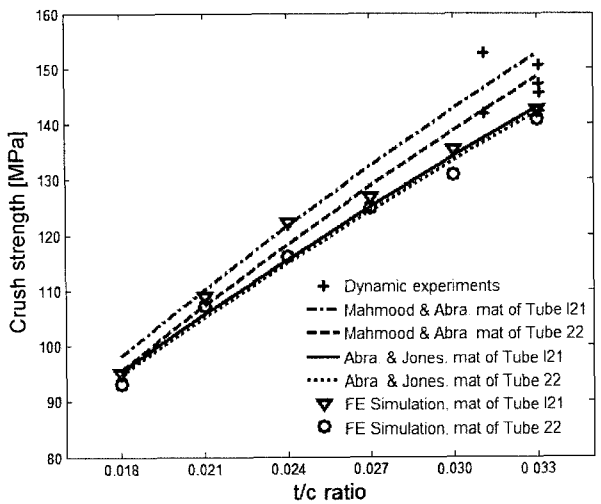

Figure 7. Crush strength of square tubes.

test, the static crush strength is bigger than expected.

Okubo *et al.* (1974) represented the dynamic crush load as a function of the static crush load and the impact velocity as:

$$P_{md}=P_{ms}\,(1.0+0.0668V) \tag{6}$$

where P_{md} is the dynamic mean crush load and V is the impact velocity. Since Okubo's experiments were performed at relatively low velocity, this equation did not well represent the results of the experiment with 10 m/s impact velocity. Therefore, Abramowicz and Jones (1984) suggested the following equation instead of equation (6).

$$\sigma_{CS}^{d}=\sigma_{CS}^{s}\,(1+0.18V^{0.256}) \tag{7}$$

where $\sigma_{CS}{}^{d}$ is the dynamic crush strength. The static crush strength calculated by equation (2) is substituted into equation (7). At an impact velocity of 10 m/s, the calculated dynamic crush strengths of Tube I21 and Tube 22 were 146.4 MPa and 148.7 MPa, respectively. When the static crush strength calculated by equation (4) was substituted into equation (7), the calculated dynamic crush strengths were 137.4 MPa for Tube I21 and 142.3 MPa for Tube 22.

Figure 7 shows the crush strength of square tubes calculated by equations (4), (5), (7) and the finite element simulations for the material condition of Tube I21 and Tube 22. The results of the analyses well approximated the experimental results and follow the functions of crush strength.

3. CONVEX AND CONCAVE TUBES

The circumferences of the section models used here are all 400 mm. Boundary conditions are as follows: all degrees of freedom at one end of the tube are fixed and a rigid body having a certain mass compressed the tube at an initial velocity of 10 m/s. Because the consecutive folding occurred relatively well compared with the previous cases of Tube I21 and Tube 22 due to the difference in the cross-section size, geometric imperfections were not used. The following two cases of Cowper-Symonds' coefficients were simulated to consider the strain rate effect.

(1) SR1–D=300/s, p=4.0, material condition of Tube I21.
(2) SR2–D=400/s, p=4.0, material condition of Tube 22.

The thickness of the tubes was varied from 1.8 mm to 3.3 mm at an interval of 0.3 mm. Different collision masses were used according to the cross-sectional area, as listed in Table 2. The mass for SR1 was decided in order for the crushed distance of the square tubes to be about 5/8 as in the case of Tube I21. For SR2, the mass was also decided in the same way, but to be about 1/3 the distance as in the case of Tube 22. Acceleration due to gravity was not considered.

Table 2. The collision mass (kg) with t/c ratio.

t/c	0.018	0.021	0.024	0.027	0.030	0.033
SR1	250	330	420	500	580	670
SR2	150	200	250	300	350	400

3.1. Shape of Convex Tubes

The shapes of the sections are shown in Figure 8. The basis section is a square section of 100 mm×100 mm. As the number of sides increased, the length of a side decreased. The longitudinal lengths of the tubes were 300 mm.

3.2. Deformation of Convex Tubes

Table 3 displays some simulation results for the convex polygonal tubes.

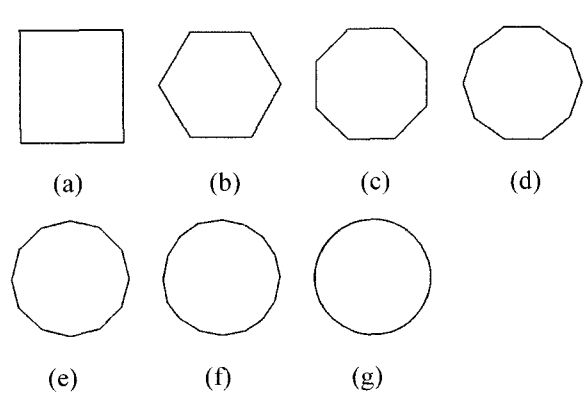

Figure 8. Shape of convex tubes: (a) 4 sides; (b) 6 sides; (c) 8 sides; (d) 10 sides; (e) 12 sides; (f) 16 sides; (g) circle.

Table 3. The simulation results for the convex tubes.

	Material	t (mm)	M (kg)	δ_f (mm)	P_m^d (kN)	CS (MPa)
4 sides	SR1	3.0	580	178	163	136
	SR2	3.3	400	108	186	141
6 sides	SR1	3.0	580	145	200	166
	SR2	3.3	400	97	207	157
8 sides	SR1	3.0	580	138	210	175
	SR2	3.3	400	91	221	167
10 sides	SR1	3.0	580	151	192	160
	SR2	3.3	400	87	231	175
12 sides	SR1	3.0	580	142	205	171
	SR2	3.3	400	84	238	181
16 sides	SR1	3.0	580	160	182	162
	SR2	3.3	400	88	227	172
Circle	SR1	3.0	580	165	176	147
	SR2	3.3	400	92	217	165

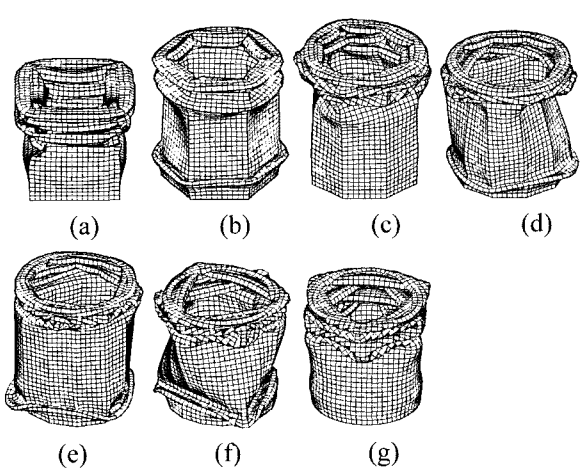

Figure 9. Deformation of convex tubes with thickness t=3.0 mm with the material condition of SR1, rigid wall mass=580 kg, and velocity=10 m/s: (a) 4 sides; (b) 6 sides; (c) 8 sides; (d) 10 sides; (e) 12 sides; (f) 16 sides; (g) circle.

3.2.1. Thickness, 3.0 mm and SR1

Figure 9 displays the collapse shapes for the convex tubes with 3.0 mm in thickness, and the material condition is the same as that of SR1. The collapse shapes are very dependent on the material properties and boundary conditions: folding of the square tube occurred stably, and as the number of sides increased, the folding of the tubes became unstable. The square tube is the most desirable for stable folding.

Figure 10 shows the rigid wall force as a function of the crushed distance of the convex tubes for t=3.0 mm.

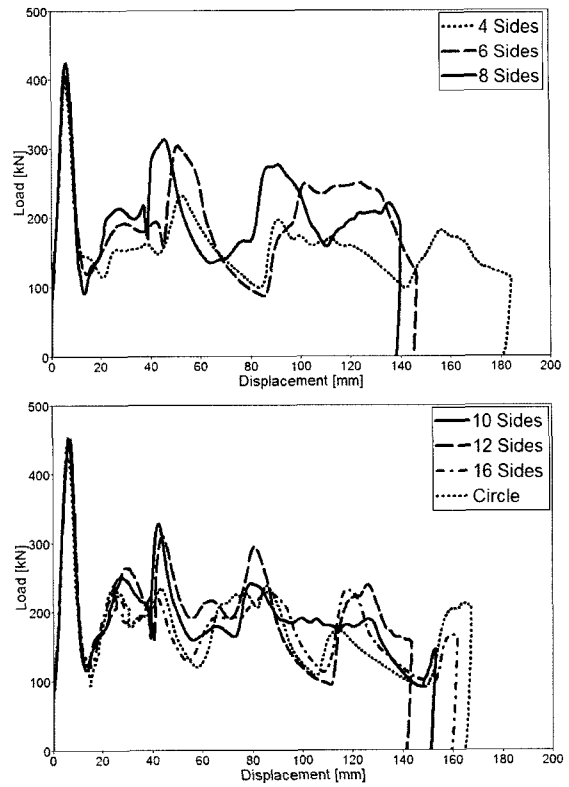

Figure 10. Rigid wall force of the convex tubes, t=3.0 mm, material condition of SR1 with the wall mass=580 kg and velocity=10 m/s.

The crushed distance of the square tube is the longest and the mean crush load is the smallest. The mean crush load of the octagonal tube is the biggest. When the number of sides is more than 10, the rigid wall force graphs are similar. This is because the mean crush load did not increase because of the unstable collapse mode when the number of sides increased.

3.2.2. Thickness, 3.3 mm and SR2

Figure 11 displays the collapse shapes when the thickness of the convex tubes is 3.3 mm and the material condition is the same as that of SR2. The square and hexagonal tubes folded relatively well. When the number of the sides was more than 8, the tubes folded asymmetrically. For this kind of unstable folding to occur, a large collapse load was required and therefore, the crushed distance was short.

Figure 12 displays the rigid wall force as a function of the crushed distance of the convex tubes for this case. When the number of the sides became more than 8, the rigid wall force graphs of the tubes were almost the same.

3.3. Shape of Concave Tubes

The circumferences of the concave tubes were 400 mm,

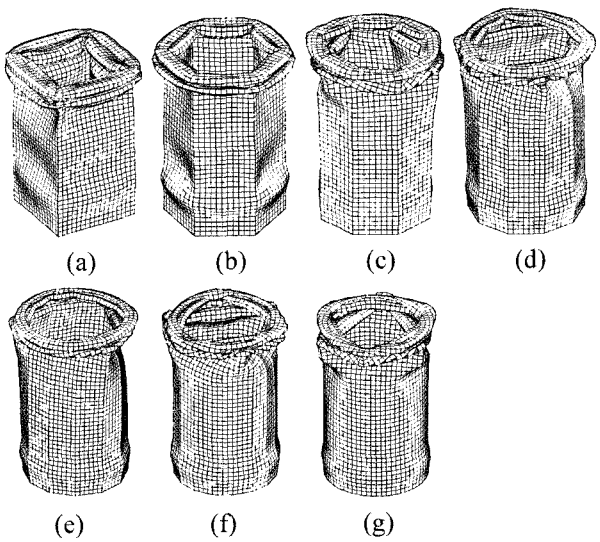

Figure 11. Deformation of convex tubes of thickness t= 3.3 mm, with the material condition of SR2, rigid wall mass=400 kg, and velocity=10 m/s: (a) 4 sides; (b) 6 sides; (c) 8 sides; (d) 10 sides; (e) 12 sides; (f) 16 sides; (g) circle.

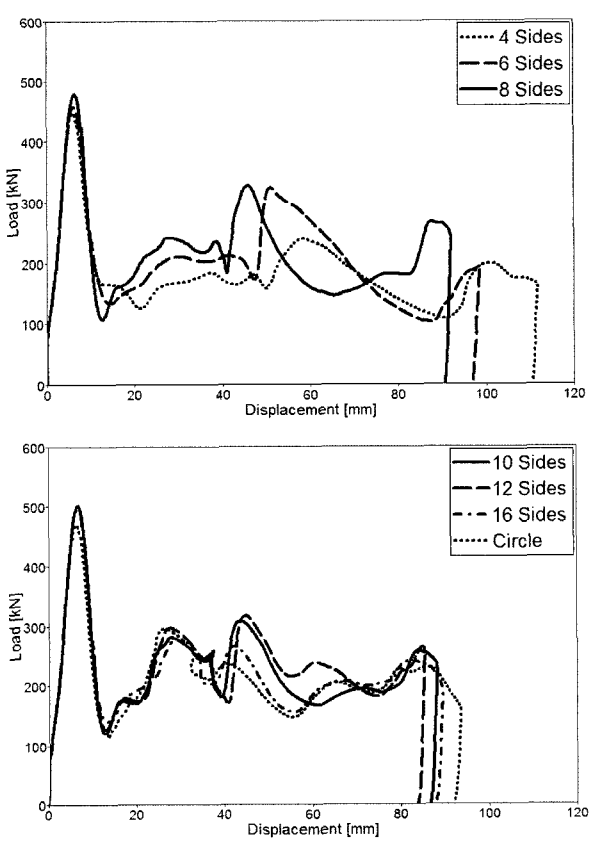

Figure 12. Rigid wall force of the convex tubes, t=3.3 mm, material condition of SR2 with the wall mass=400 kg and velocity=10 m/s.

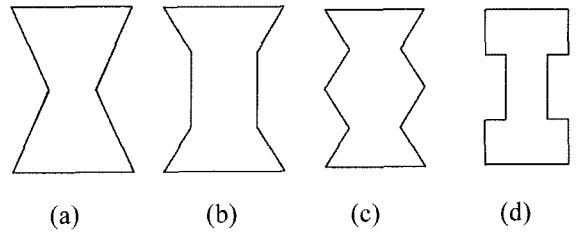

Figure 13. Shape of concave tubes: (a) 6 sides; (b) 8 sides; (c) 10 sides; (d) 12 sides.

Table 4. The results for the concave tubes.

	Material	t (mm)	M (kg)	δ_f (mm)	P_m^d (kN)	CS (MPa)
6 sides	SR1	3.0	580	177	164	136
	SR2	3.3	400	104	192	145
8 sides	SR1	3.0	580	161	181	150
	SR2	3.3	400	98	204	154
10 sides	SR1	3.0	580	149	194	162
	SR2	3.3	400	88	228	173
12 sides	SR1	3.0	580	132	219	183
	SR2	3.3	400	76	262	198

as they were in the case of the convex tubes. The shapes of the sections are shown in Figure 13. The basis section is the rectangular section 120 mm in length×80 mm in width. As the number of sides increased, the area of the section decreased. The longitudinal lengths of the concave tubes were all 300 mm as before.

3.4. Deformation of Concave Tubes

Table 4 displays some simulation results for concave polygonal tubes.

3.4.1. Thickness, 3.0 mm and SR1

Figure 14 displays the collapse shapes when the thickness of the concave tubes is 3.0 mm and the material condition is the same as that of SR1. When the number of sides was

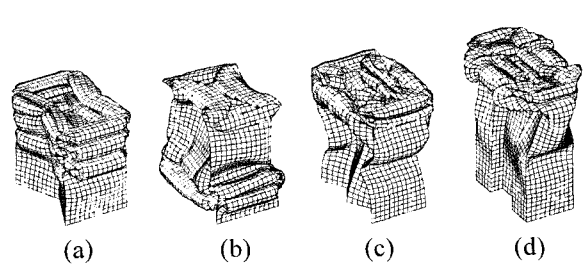

Figure 14. Deformation of concave tubes, t=3.0 mm, material condition of SR1 with rigid wall mass=580 kg and velocity=10 m/s: (a) 6 sides; (b) 8 sides; (c) 10 sides; (d) 12 sides.

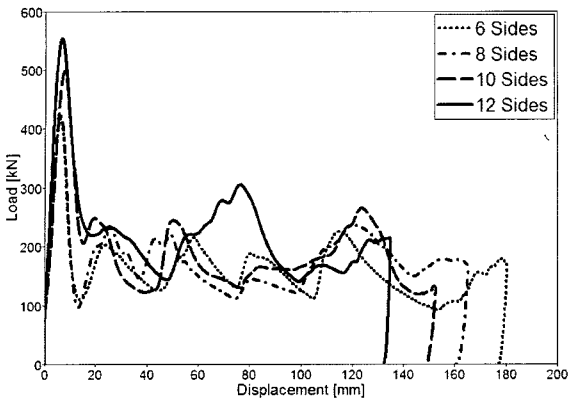

Figure 15. Rigid wall force of the concave tubes, t=3.0 mm, material condition of SR1 with rigid wall mass=580 kg and velocity=10 m/s.

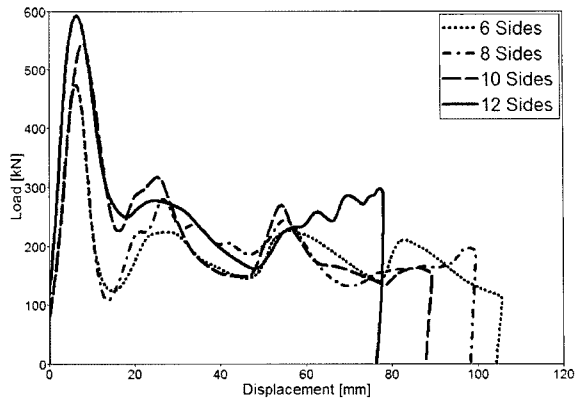

Figure 17. Rigid wall force of the concave tubes, t=3.3 mm, material condition of SR2 with rigid wall mass=400 kg and velocity=10 m/s.

6, the most stable folding occurred. Because the crushed distance was the shortest in the I-type tube with 12 sides, the mean crush load of I-type tube was the biggest.

Figure 15 shows the rigid wall force versus the crushed distance when the thickness of concave tubes is 3.0 mm for the same material condition as that of SR1 and a rigid wall mass of 580 kg. As the number of sides increased, the crushed distance proportionally decreased. When the crushed distance shortened, the mean crush load increased, because all the tubes absorbed the same kinetic energy. Since the crushed distance of the I-type tube was the shortest among the tubes, the mean crush load was the largest.

3.4.2. Thickness, 3.3 mm and SR2

Figures 16 and 17 show the collapse shapes and crush loads of the concave tubes with 3.3 mm in thickness and the material condition of SR2. The most stable folding occurred when the number of sides was 6, as in the case for t=3.0 mm. The crushed distance also became short in proportion to the number of sides. Because the crushed distance of the I-type tube was the shortest, the mean crush load of the I-type tube was the biggest.

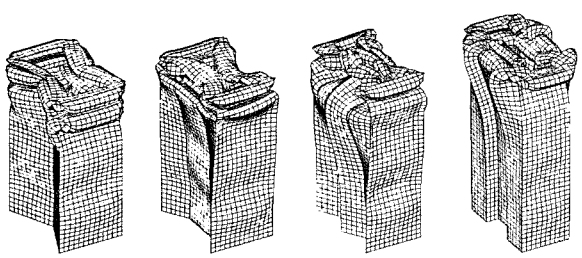

(a) (b) (c) (d)

Figure 16. Deformation of concave tubes, t=3.3 mm, material condition of SR2 with rigid wall mass=400 kg and velocity=10 m/s: (a) 6 sides; (b) 8 sides; (c) 10 sides; (d) 12 sides.

3.5. Crush Strength

Figure 18 displays the mean of the crush strength for material properties of SR1 and SR2 as a function of the number of sides. In most cases, the crush strength increased as the thickness increased. Also, the crush strength increased with an increased the number of sides. However, the crush strength of convex tubes decreased when the number of sides was more than 10 because the collapse mode became unstable as the number of sides increased. When the t/c ratio was below 0.024, the hexagonal tube showed good performance. The crush strength of the hexagonal tube increased by about 20% more than the crush strength of the square tube. When the t/c ratio was more than 0.027, the octagonal tube showed good result. The crush strength of the octagonal tube increased by about 25% more than the crush strength of the square tube. Of the concave tubes, the crush strength of the I-type tube was the highest, regardless of the

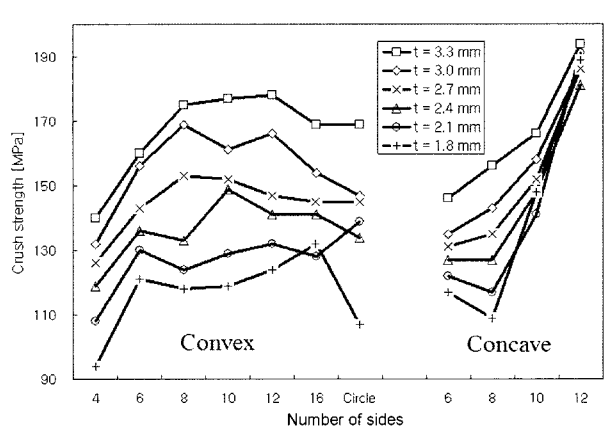

Figure 18. Mean of the crush strengths relative to the number of sides.

thickness considered. Therefore, the I-type tube is the most desirable section shape for a thin tube. The crush strength of the I-type tube appeared to be about 50% higher than the crush strength of the square tube.

4. CONCLUSION

The dynamic collapse simulation demonstrated significant effects of strain rate on tubes. Among the various methods to account for the strain rate effect, we used the Cowper-Symonds model. The Cowper-Symonds' coefficients that produced the closest results to that of the experimental results were chosen: 300~500/s for D and 4~5 for p.

The modified coefficients were applied in the numerical collapse simulation of 11 types of thin-walled polygon tubes: 7 convex polygon tubes and 4 concave polygon tubes. The simulation results show that the thin hexagonal tube and the thick octagonal tube gave relatively good performance of the convex polygon tubes. The crush strengths of the hexagonal and octagonal tubes increased by about 20% and 25% over that of the square tube, respectively. Among the concave tubes, the I-type tube gave the best performance. Its crush strength was about 50% higher than that of the square tube. To obtain the desired crush strength, the amount of material used in the I-type tube can be reduced to half of that of the square tube.

This study mainly focused on the analysis of several section shapes of tubes as longitudinal members without considering manufacturing. Accordingly, some of the outcomes in this research may not be directly applicable to real vehicles because of the limitations in manufacturability, fabrication cost, and so on. From the practicality viewpoint, further research is required in this field in terms of the producibility of the section shapes mentioned, including a spot-welded double-hat section.

REFERENCES

Abramowicz, W. and Jones, N. (1984). Dynamic axial crushing of square tubes. *Int. J. Impact Engng.* **2, 2,** 179–208.

Abramowicz, W. and Wierzbicki, T. (1983). On the crushing mechanics of thin-walled structures. *J. Applied Mechanics,* **50,** 727–734.

Abramowicz, W. and Wierzbicki, T. (1989). Axial crushing of multicorner sheet metal columns. *J. Applied Mechanics,* **56,** 113–120.

Gonzalez, M., Chitoor, K., Kim, H. S. and Tyan, T. (2005). Testing and modeling of metalic multicorner columns in axial crush. *SAE Paper No.* 2005-01-353.

Kang, W. J. and Huh, H. (2000). Crash analysis of autobody structures considering the strain-rate hardening effect. *Int. J. Automotive Technology* **1, 1,** 35–41.

Kim, S.-K., Im, K.-H., Hwang, C.-S. and Yang, I.-Y. (2002). A study on experimental characteristic of energy absorption control in thin-walled tubes for the use of vehicular-structure. *Int. J. Automotive Technology* **3, 4,** 137–145.

Mahmood, H. F. and Paluszny, A. (1981). Design of thin walled columns for crash energy management – Their strength and mode of collapse. *SAE Paper No.* 811302.

Mamalis, A. G., Manolakos, D. E., Ioannidis, M. B., Kostazos, P. K. and Dimitriou, C. (2003). Finite element simulation of the axial collapse of metallic thin-walled tubes with octagonal cross-section. *Thin-Walled Structures,* **43,** 1646–1661.

Ohkubo, Y., Akamatsu, T. and Shirasawa, K. (1974). Mean crushing strength of closed-hat section members. *SAE Paper No.* 740040.

Otubushin, A. (1998). Detailed validation of an non-linear finite element code using dynamic axial crushing of a square tube. *Int. J. Impact Engng.* **21, 5,** 349–368.

Rossi, A., Fawaz, Z. and Behdinan, K. (2005). Numerical simulation of the axial collapse of thin-walled polygonal section tubes, *Thin-Walled Structures,* **43,** 1646–1661.

Yamashita, M., Gotoh, M. and Sawairi, Y. (2003). Axial crush of hollow cylindrical structures with various polygonal cross-sections numerical simulation and experiment. *J. Materials Processing Technology,* **140,** 59–64.